Suppression of Sn whisker growth from SnAgCu solder alloy with TiO_2 and ZnO reinforcement nano-particles by increasing the corrosion resistance of the composite alloy

Balázs Illés[1),2)], Halim Choi[1)], Tamás Hurtony[1)], Karel Dusek[2)], and David Busek[2)] Agata Skwarek [3)4)]

[1)] Budapest University of Technology and Economics, Faculty of Electrical Engineering and Informatics, Department of Electronics Technology, Budapest, Hungary

[2)] Department of Electrotechnology, Faculty of Electrical Engineering, Czech Technical University in Prague, Prague, Czech Republic

[3)] Łukasiewicz Research Network - Institute of Microelectronics and Photonics, LTCC Technology and Printed Electronics Research Group, Kraków, Poland

[4)] Gdynia Maritime University, Department of Marine Electronics, Gdynia, Poland

e-mail: illes.balazs@vik.bme.hu

Abstract:

The main joining process of the electronic industry is still soldering with different alloys of Sn. This work studied the relationship between Sn whisker growth and corrosion resistance of 99Sn0.3Ag0.7Cu-TiO_2/ZnO (0.25wt%) composite solder alloys in a corrosive environment via scanning electron microscopy and focused ion beam techniques. The corrosive environment test showed that the application of TiO_2 and ZnO nano-particles almost totally suppressed the Sn whisker growth and improved the corrosion resistance of the composite solder alloys compared to the reference 99Sn0.3Ag0.7Cu alloy. The microstructural analysis of the reference 99Sn0.3Ag0.7Cu solder alloy showed that the volumetric increase of the corroded β-Sn grains resulted in local mechanical stress in the solder joints, which was released by Sn whisker development. However, in the composite solder joints, the increased grain boundary fraction and segregation of the TiO_2 and ZnO nano-particles to the grain boundaries resulted in a relatively uniform and compact protective oxide layer at the β-Sn grain boundaries. This suppressed the formation of SnO_x, and via this, the corrosion-induced whisker growth.

Keywords: Sn whisker; composite alloy; soldering; ceramic nano-particles; localized corrosion.

1. Introduction

The main joining process of electronic components is still soldering. Therefore the quality and reliability of solder joints is a key point in the failure-free operation of the equipment. After

the lead-free soldering technology implementation, the next milestone was the reduction of the silver (Ag) content in the widely applied SnAgCu solder alloys [1]. Ag is more and more expensive, and moreover, high Ag content in the solder alloy (over 2.8wt%) can cause thermo-mechanical problems. Generally used SnAgCu alloys, SAC305 (Sn96.5Ag3Cu0.5) and SAC405 (Sn95.5Ag4Cu0.5), exceed this critical Ag level. A fast cooling rate (below around 1.5 K/s) during soldering might result in the formation of large, brittle, plate-like Ag_3Sn intermetallic compounds (IMCs) in the solder bulk, which can cause shrinkage defects [2]. Such a solder joint will be sensitive to thermo-mechanical or even to simple mechanical loads, e.g., dropping, which is frequent in the case of any mobile devices.

Promising low Ag content alloys are the SAC0307 (Sn99Ag0.3Cu0.7) and SAC105 (Sn98.5Ag1Cu0.5); they are already used in the industry, but the SAC305 is still dominant. However, in the low Ag content alloys, the higher Sn content might result in reliability risks like Sn whisker growth [3]. Sn whiskers are surface defects on pure or high tin content objects like solder joints or surface finishes. Their typical length is between 20 and 100μm, but sometimes it can reach even a millimeter length. Therefore, the whisker phenomenon means a serious reliability risk in modern microelectronics because of the possible short circuits between the fine pitch leads of the components. The driving force of the whisker growth on the Sn surfaces is always some kind of mechanical stress on the Sn grains. This mechanical stress could originate from residual stress due to the process of the Sn object (soldering or surface plating); from thermo-mechanical effects (e.g., thermal expansion); from other volumetric changes caused by oxidation or intermetallic formation; or from simple direct mechanical load [4].

It has been known for a decade that the SAC305 solder alloys can develop whiskers [5]. But unfortunately, in a corrosive environment, the low Ag content solder alloys (like SAC0307) could be even more sensitive to whiskers growth than the generally used SAC305 due to their lower corrosion resistance [6, 7]. There are two main types of Sn whiskers, the nodule-like whiskers and the filament-like whiskers. The nodule whisker is always shorter, twisted, and polycrystalline, while the filament is long, straight, and monocrystalline [7]. A straightforward solution could be to reduce the whisker susceptibility with some kind of alloying. Hua and Yang [8] reached the opposite results by doping SAC alloys with Zn and In, namely that the doping decreased the corrosion resistance of the alloy and increased whisker susceptibility. Cao et al. [9] had got similar results in the case of Zn addition. Illés et al. [10] could delay the whisker growth by alloying 1wt% Bi into SAC0307 solder alloy in the case of thin-film layers because the Bi addition could decrease the bulk modulus of the layer; furthermore, the Bi addition

decreased the number of long filament whiskers. Delhaise et al. [11] observed a similar effect of the Bi addition into SAC305 solder alloy. Mohanty and Lin [12] could increase the corrosion resistance and decrease of whiskering of SAC105 solder alloy by alloying Ni.

A novel trend in solder alloys development is the use of ceramics as reinforcement in the solder joints. It means that ceramic particles are mixed into the solder paste in 0.05 – 1 wt%. The reinforcing particles should be small-sized and form self-organized dispersive systems, which promote heterogeneous nucleation [14]. Therefore, the ceramic nano-particles (NPs) are usually applied. Their size is usually below 100nm. Their application results in a so-called composite or nano-composite solder alloy [13]. A wide range of ceramic particles has already been tried as reinforcement for solder alloys, like TiO_2, ZnO, SiC, ZrO_2, Al_2O_3, Fe_2O_3, Si_3Ni_4, La_2O_3 [14–18]. Usually, the reinforcements positively affect the quality of the solder joints. Although the non-soluble NPs may slightly increase the liquidus temperature of the composite alloy (of about 1-2K) [19].

The most important effect of the reinforcement particles is that they modify the thermal and mechanical parameters of the solder joints [20, 21] via grain refinement and the modified grain boundary/interfacial characteristics [22, 23]. In the case of SnAgCu systems, the solder joint is built up from β-Sn grains, Cu_6Sn_5, Cu_3Sn, and Ag_3Sn IMC grains. The non-soluble NPs incorporate at the grain boundaries into the solder matrix [24, 25]. They suppress the grain growth (in the case of β-Sn grains and IMC as well) and retard the dislocation motion leading finally to solder joint strengthening [26, 27]. The microstructural result is a refined β–Sn matrix, smaller IMC particles with increased interphase spacing in the solder bulk, and a thinner and finer IMC layer at the Sn–Cu soldering interface [24, 28]. These phenomena cause the hardening of the β–Sn matrix [29], an increase of the tensile [24] and yields strength [30, 31], and improvement of the microhardness [24]. Furthermore, the NP reinforcements can decrease the coefficient of thermal expansion, which results better thermal fatigue reliability [21].

The previously discussed, mainly mechanical improvements of the solder joints, are very important from the quality aspects of the solder joints. However, the possible reliability effects of the NP reinforcements on the composite solder joints have not been widely studied. The refined microstructure of the composite solder joints could have effects on reliability issues. Our aim in this study was to investigate the effect of TiO_2 and ZnO NP reinforcements on the corrosion resistance and Sn whisker susceptibility of composite solder joints.

2. Materials and Methods:

Standard SAC0307 (Sn99Ag0.3Cu0.7, Alpha Industries) solder paste was reinforced by the addition of TiO_2 (Sigma-Aldrich 718467) and ZnO (Sigma-Aldrich 677450) ceramic NPs in 0.25 wt%. The 0.25wt% reinforcement was selected because composite solder alloys usually showed the best soldering / mechanical performance with this amount of reinforcement [27]. The primary particle size of the TiO_2 NPs was 21 nm, according to the transmission electron microscopy analysis of the manufacturer. The particle size of the ZnO NPs was <50 nm (according to BET surface area analysis of the manufacturer). A planetary ball-mill was used to mix the NPs homogeneously into the solder paste. Altogether, three different solder compositions (solder pastes) were investigated: reference SAC0307, SAC0307-TiO2 (0.25wt%) and SAC0307-ZnO (0.25wt%).

From the solder pastes, solder joints were fabricated by classical surface mounting technology (SMT). The solder pastes were printed on test printed circuit boards (PCBs) by screen printing with a 125 μm thick stainless steel stencil foil. The PCBs were made from a standard 1.6mm thick FR4 laminate covered with 35μm thick Cu foil. Solder pads were formed from the Cu foil which was covered by immersion silver (Ag) surface finishing. Each test board contained 50 pcs 0603 sized (1.5 x 0.75 mm) SMD chip resistor, which was placed by a manual pick & place machine into the solder deposits. The solder paste was melted (reflowed) in an infrared (IR) heated batch oven. Linear reflow profile was applied with the following main parameters: preheating (up to 150˚C, from 0s to100s), soak (between 150-200˚C, from 100s to 280s), ramp-up (up to 250˚C, from 280s to 350s).

The samples were loaded with a thermal-humidity (TH) test 85ºC/85RH% for 4000h to enhance whisker growth. The corrosive environment effectively induces whisker growth from solder joints [6]. The surface of the solder joints was investigated after every 500 hours by a FEI Inspect S50 Scanning Electron Microscopy (SEM) using a thermal emission gun. The axial length of Sn whiskers was measured according to the JESD201 standard, which defines the whisker length between the tip of the whisker and the surface (see in more detail in [32]). The number of Sn whiskers and average lengths were calculated in the function of time on ten individual solder joints (means ten samples). Surface cuts were prepared on the solder joints in order to observe the microstructure under and around the developed Sn whiskers by a Thermo Scientific Scios 2 type Focused Ion Beam (FIB) device. Deeper microstructural investigations of the whisker roots were carried out by a Thermo Scientific Scios 2 type Scanning Electron Microscopes having non-immersion field emission gun and Energy Dispersive X-ray spectroscopy (EDS).

3. Results

Fig. 1 shows the surface changes of a reference SAC0307 solder joint during the 4000 hours of TH test. The solder joints were covered with a massive flux residue layer after the soldering process (Fig. 1.a), which was removed by vibration cleaning in isopropyl alcohol. In the middle of the solder joint, a large Cu_6Sn_5 IMC network was visible (Fig. 1.b-f), which means that the IMC pikes reached the surface of the solder joint. Darker grey spots appeared on the surface of the sample at 1000h (Fig. 1.b), which were growing and spreading during the test (Fig 1.c-f). The contrast difference means an elemental difference in the SEM-BSE micrograph. It was proven by EDS measurements that the darker spots contain a much higher amount of oxygen than their surroundings, so the spots were corrosion spots (SnO or SnO_2, marked by SnO_x).

The first Sn whiskers were found at 1500 hours at the upper corner of the solder joint (Fig. 1.c). They formed directly next to a corrosion spot. They were nodule type, and their length was between 2-4 μm. After 2000 hours of TH test, much more corrosion spots were visible at the upper part of the solder joint (Fig. 1.d), and the number of whiskers grew as well. Up to 3000 hours, the corroded areas started join together, and the number of whiskers grew considerably (Fig. 1.e); some of them reached 20-40 μm in length. At the end of the TH test, the upper part of the solder joint was covered by an almost continuous thick corroded area and plenty of Sn whiskers (Fig. 1.f). Almost only nodule-type whiskers were found on the reference sample, which is usual in the case of SnAgCu solder alloys [6, 7].

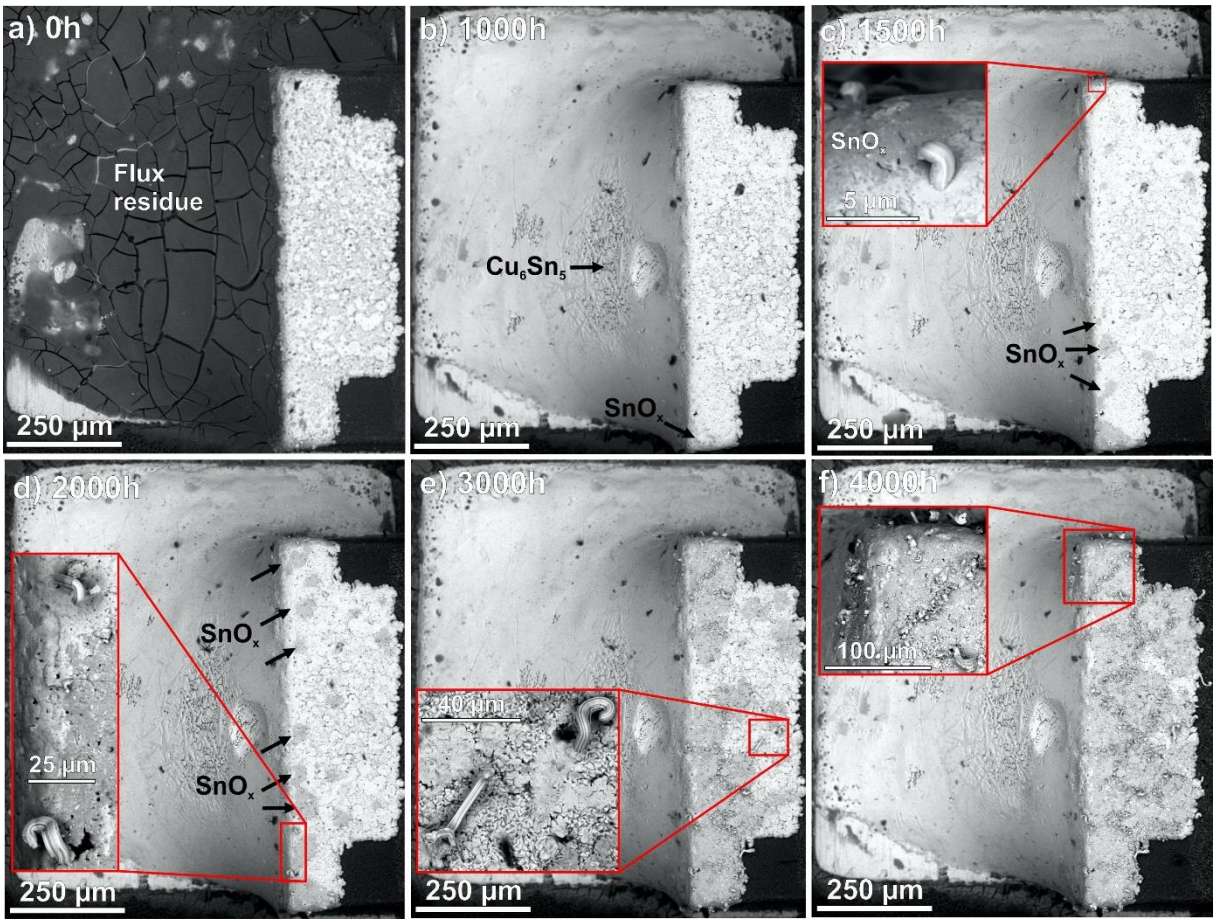

Fig. 1. SEM-BSE micrograph about the surface of a reference SAC0307 solder joint during the TH test: a) 0h; b) 1000h; c) 1500h; d) 2000h; e) 3000h; f) 4000h.

Although it seems that only the upper part of the solder joint was corroded and prone for Sn whisker formation, a tilted SEM micrograph of the solder joint (made by a field-emission electron gun) shows that the corrosion was not limited to the upper part of the solder joint (Fig. 2). The lesions of the surface were considerable. Corrosion products and Sn whiskers (marked by red circles) are visible on the surface of the solder joint (Fig. 2). Probably the upper (horizontal) part of the solder joint kept the condensed water more than the lower (non-horizontal) part, and it caused more serious corrosion there. The Cu_6Sn_5 crystal network in the middle of the meniscus (which was visible in Fig. 1 as well) was not the result of the aging test.

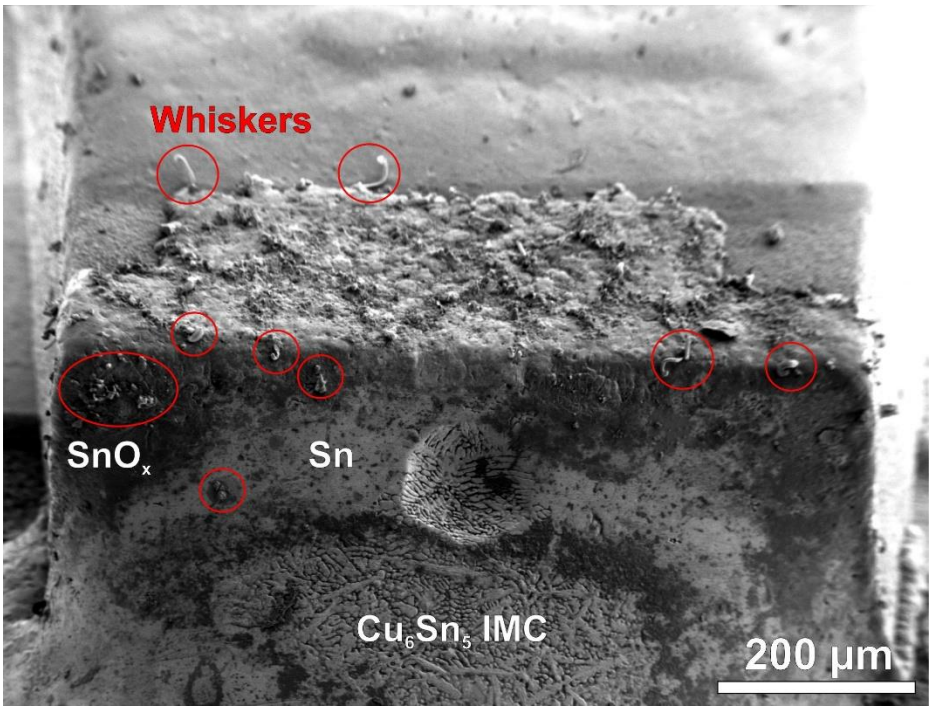

Fig. 2. SEM-BSE micrograph of a reference SAC0307 solder joint, after 4000h TH test.

Fig. 3 shows the surface of SAC0307-TiO_2 (0.25wt%) and SAC0307-ZnO (0.25wt%) composite solder joints after 4000 hours of TH test. The differences between the surfaces of the reference SAC0307 (Fig. 1.f) and the composite solder joints (Fig. 3) were considerable. In the case of the composite solder joints, only some marks of corrosion were found after 4000h of corrosive TH test. Around these corrosion spots, a few short whiskers grew (Fig. 3.c-e), but all of them developed only after 3500 hours. The first corrosion spots appeared at 2000h in the case of TiO_2 samples and at 2500h in the case of ZnO sample. These results suggest that the nano-particles could increase the corrosion resistance of the composite solder joints significantly compared to the reference SAC0307 alloy. With the suppressed corrosion, the whisker growth also decreased considerably in the case of the composite solder joints.

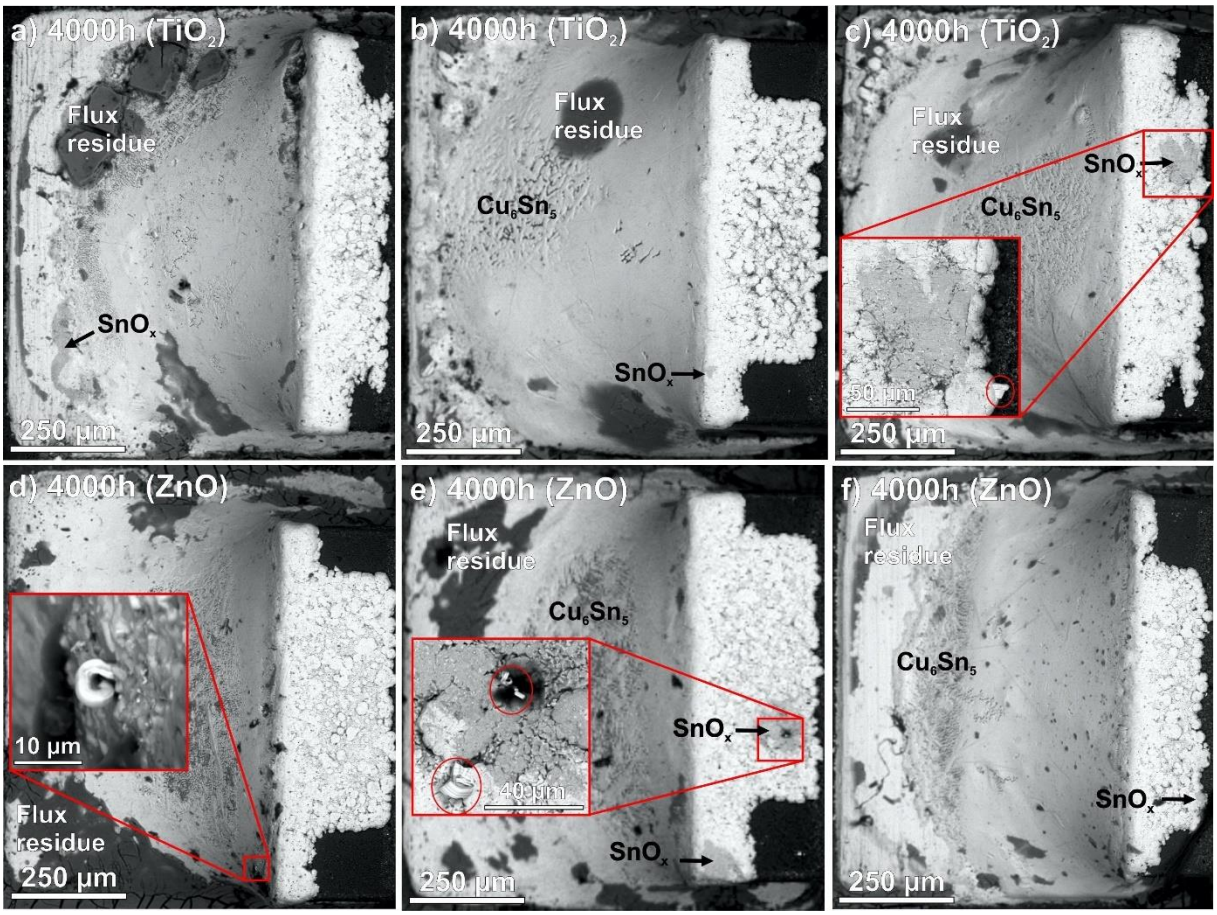

Fig. 3. SEM-BSE micrographs of 3-3 SAC0307-TiO_2 (0.25wt%) and SAC0307-ZnO (0.25wt%) composite solder joint after 4000h TH test: a) TiO_2 (1); b) TiO_2 (2); c) TiO_2 (3); d) ZnO (1); e) ZnO (2); f) ZnO (3).

The statistical results (number of Sn whiskers and the average Sn whisker lengths) can be seen in Fig. 4.

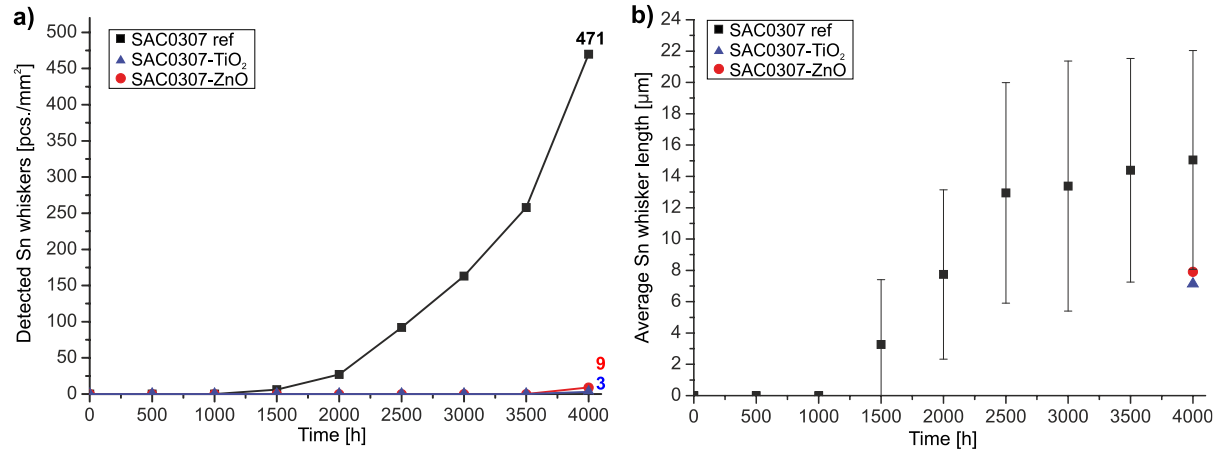

Fig. 4. Sn whisker statistics: a) number of detected Sn whiskers; b) average lengths of the Sn whiskers.

The characteristics of the whisker growth on the reference SAC0307 samples followed the usual characteristics in the case of a corrosive environment [6, 7]. It means that after the first appearance (at 1500h), the number of the Sn whiskers showed an exponential increase, but saturation was not reached till 4000 hours of TH test (Fig. 4.a). Altogether, 471 Sn whiskers were found on the reference samples. Although the average length of the Sn whiskers increased during the whole TH test, it reached saturation at 2500h; after it the length increase was marginal. Probably the intensive oxidation, which affected the whisker as well, blocked their further length increase. As it was discussed above, most of the detected Sn whiskers were nodule-type; therefore, the average length barely reached 15 μm till the end of the study. The deviation was considerable, between 6-7 μm, but it is usual in case whisker studies [6, 10]. The longest detected Sn whisker was 50 μm.

In the case of the SAC0307-TiO_2 and SAC0307-ZnO samples, only a few Sn whiskers were found. Their average lengths were ~7 μm, but this data is not representative due to the very low amount of samples (the standard deviations were not calculated due to the same reason). Consequently, the TiO_2 and ZnO NP reinforcements were very effective in increasing the corrosion resistance of the solder joints and suppressing the Sn whisker growth.

4. Discussion

Fig. 5. shows a nodule whisker couple (and their analysis results) that grew on a reference SAC0307 solder joint. The length of the whiskers was between 25-40 μm, and they had 7-8μm diameter (Fig. 5.a). The root of the whiskers (marked by red rectangular in Fig. 5.a) was cut by Ga ion beam to investigate its' microstructure. Fig. 5.b shows the SEM-SE micrograph of the whisker root. Some Kirkendall voids are barely visible under the whisker structure, which is a usual phenomenon due to Sn atoms transport during the whisker growth. The SEM-BSE micrograph revealed a considerable contrast difference at the whisker root (Fig. 5.c). The EDS results (Fig. 5.d) proved that the right darker gray grain(s) under the whisker was highly corroded (EDS showed an increased amount of oxygen there) while the left brighter gray grain(s) remained mostly Sn. The grain boundary of the corroded and non-corroded area is marked by the red lines in Fig. 5.c. The contrast difference appeared on the surface of the whisker as well, which means that even the surface of the whisker is covered by SnO_x. This proves our preconception that the oxidation of the whiskers could slow down their length increase.

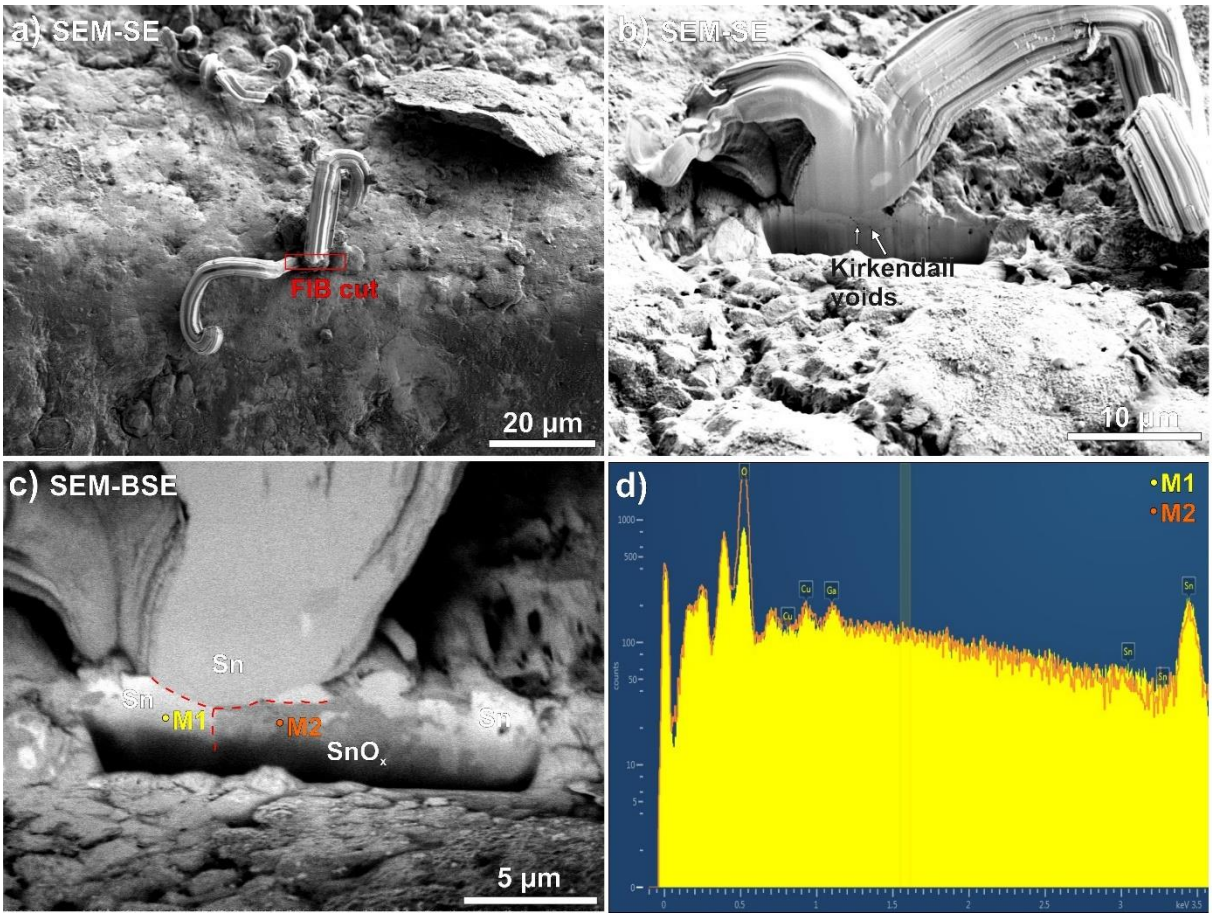

Fig. 5. Sn whisker couple on the SAC0307 solder joint: a) nodule Sn whiskers; b) SEM-SE micrograph of the FIB cut at the root of the whiskers; c) SEM-BSE micrograph of the FIB cut at the root of the whiskers; d) EDS result of the Sn grains at the root of the whisker.

Fig. 6 shows another FIB cut under a nodule whisker on a SAC0307 solder joint after 4000 hours TH test. The length of this whisker was between ~10-25 µm, and it had a diameter between 5-7µm. The root of the whisker was cut by Ga ion beam to investigate its' microstructure. Some Kirkendall voids were also found under this whisker too. The SEM-BSE micrograph also showed considerable elemental contrast under this whisker (Fig. 6). The β-Sn grain(s) on the left side was highly corroded, while the right side remained mostly Sn, similarly to the previous sample (Fig. 5). The grain boundary of the corroded and non-corroded areas is marked by the red lines in Fig. 6.

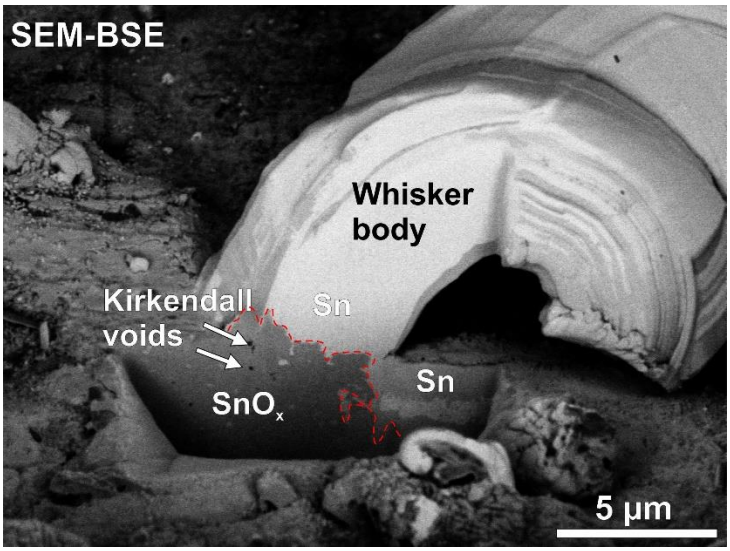

Fig. 6. SEM-BSE micrograph of the FIB cut at the root of a whisker on a SAC0307 solder joint.

Sn-Cu alloys with TiO_2 particles, and generally, most of the composite coatings are usually characterized by improved wear- and corrosion resistance [33]. To be able to explain the corrosion resistance increase of our composite solder alloys, the followings need to be considered: the corrosion process of Sn; the relationship between the solder microstructure and the corrosion; and the relationship between ceramic NPs and corrosion. First, investigate the corrosion behavior of SAC alloys.

Table 1 shows the standard Gibbs free energies and the equilibrium reduction potentials of the Sn oxides.

Table 1. Standard Gibbs free energies and equilibrium reduction potentials of tin oxides, data from [34].

Oxide	Free energy of formation, ΔG^0 [kJ/mol], at 298K	Equilibrium potential [V]
SnO	-251.9	-0.7955
SnO_2	-515.8	-0.8266
$Sn(OH)_{2(aq)}$	-491.6	-0.8090
$Sn(OH)_{4(aq)}$	-994.9	-0.8406

When ΔG^0 is negative, a process will proceed spontaneously, and in an electrochemical cell, each chemical species will move from areas with higher electrochemical potential to areas with

lower electrochemical potential. So, according to Table 1, the formation of all of the listed oxides is possible. The formation of SnO and SnO_2 is described with the following equations:

$$Sn + H_2O \rightarrow SnO + 2H^+ + 2e^- \quad (1)$$

$$Sn + 2H_2O \rightarrow SnO_2 + 4H^+ + 4e^- \quad (2)$$

In normal circumstances, only a thin (some nm thick) Sn-oxide layer develops on the surface of the Sn objects. However, in a wet environment, in the case of SAC alloys, excessive localized corrosion can occur as well, which produces non-uniform and locally thick layer of Sn-oxide (as was found in Fig. 5 and 6). Localized corrosion takes place wherever anodic and cathodic sites on a metal surface can be distinguished, usually due to heterogeneities either in the material or in the environment to which a material is exposed. The standard reduction potential of Sn is below the IMCs (Cu_6Sn_5, Cu_3Sn, and Ag_3Sn) [35], so Sn is anodic to the IMCs inside the solder joints. Furthermore, during the TH test, the condensed water film with possible contaminants like Cl, S, or Na forms an electrolyte layer on the solder joints. Therefore the corrosion of the solder joints could accelerate inwards in the layer [36] (as it was found in Fig. 5 and 6).

In the electrolyte layer, the corrosion and dissolution process occurs preferably at β-Sn grains, Eq. (3-4) [35]. The depolarization process of the oxygen is the parallel reaction at the cathode, Eq.(5). The corrosion products forms when Sn^{2+}/Sn^{4+} meets with the OH^- form the cathode and they precipitates ($KSP(Sn(OH)_4) = 10^{-57}$ and $KSP(Sn(OH)_2) = 10^{-27}$) [37] according to Eq. (6)–(9) [38]:

$$Sn \rightarrow Sn^{2+} + 2e^- \quad (3)$$

$$Sn^{2+} \rightarrow Sn^{4+} + 2e^- \quad (4)$$

$$2H_2O + O_2 + 4e^- \rightarrow 4OH^- \quad (5)$$

$$Sn^{2+} + 2OH^- \rightarrow Sn(OH)_2 \quad (6)$$

$$Sn^{4+} + 4OH^- \rightarrow Sn(OH)_4 \quad (7)$$

$$Sn(OH)_2 \rightarrow SnO + H_2O \quad (8)$$

$$Sn(OH)_4 \rightarrow SnO_2 + H_2O \quad (9)$$

The application of NP reinforcements like TiO_2 or ZnO generally refines the β-Sn network, which means a much smaller grain in the composite solder joint than in the basic SACs [27-29]. FIB cuts were prepared on the surface of the solder joints right after the soldering to observe the grain structures. Fig. 7.a shows the grain structure of a reference SAC0307 solder joint. Only three large grains were distinguished on the 15 x 30 μm area of the FIB cut, which means 15-20 μm grain size. Fig. 7.b shows the grain structure of a SAC0307-TiO_2 composite solder

joint, which was considerably refined. On a FIB cut with a similar area (15 x 30 µm), 30-35 grains were found, which means 3-8 µm grain size. Fig. 7.c is an SEM-SE micrograph with a higher magnification of the SAC-TiO_2 samples, which shows the incorporation of the TiO_2 NPs at the grain boundaries. The results were confirmed by EDS as well (Fig. 7.d) The NPs were distributed homogeneously without agglomeration.

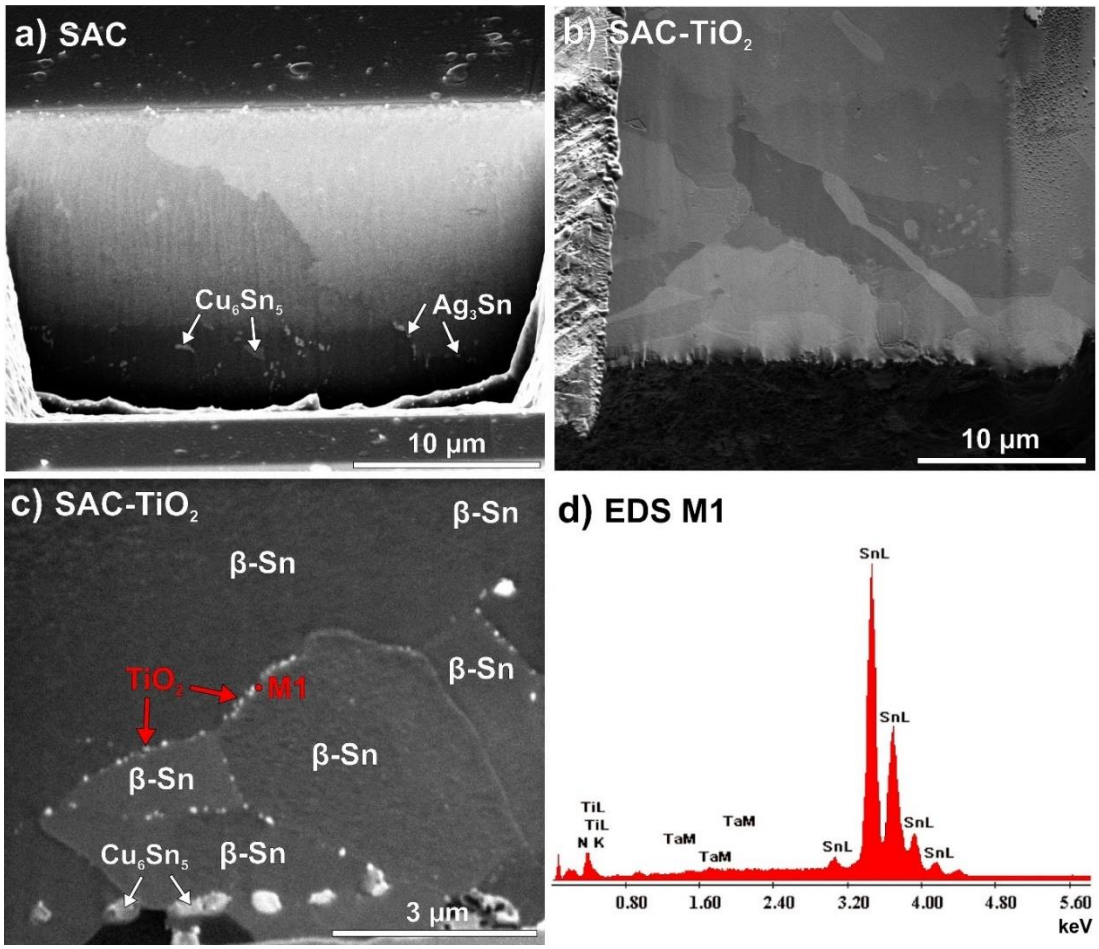

Fig. 7. The grain structure of the solder joints: a) SEM-SE micrograph of SAC0307; b) SEM-SE micrograph of SAC0307-TiO_2; c) higher magnification SEM-SE micrograph of SAC0307-TiO_2; d) EDS of M1 measurement point.

The corrosion process prefers to start along the grain boundaries, and usually, higher corrosion rates are observed in the case of materials with a higher surface free energy [39]. The refined grains of the composite solder joints (Fig. 7.b) result in an extensive grain boundary network, which has much higher grain-boundary free energy than the reference SAC has [40]. Therefore the composite solder joints with a smaller grain size should promote an accelerated formation of the oxide corrosion product layer, as it was approved several times by Gupta and Srivastava as well [39, 41, 42]. However, we observed oppositely that the composite solder

joints performed much better corrosion resistance than the reference one, which could be explained only by the role of the incorporated NPs at the grain boundaries of the composite solder joints (Fig. 7.c).

The findings of Lala et al. [43] were very similar to our observations. They tried to increase the corrosion resistance of Sn coatings by adding 1.3wt% Cr. They found that the incorporation of a minor amount of Cr leads to a considerable increase in the corrosion resistance property (40% reduction in the corrosion current density) of Sn coatings. They explained their results with the following: that incorporating Cr into the Sn matrix also caused Sn grain refinement; but it increased in high angle grain boundary fraction to help segregation of Cr at the grain boundaries to reduce strain in the grains [43]. In a corrosive environment, the large grain boundary area fraction with Cr segregation results in the formation of a protective Cr-oxide layer at the grain boundaries. The addition of Cr might act very similarly to TiO_2 or ZnO NPs, since Cr is also badly soluble in the Sn matrix, so it is incorporated mostly at the grain boundaries [44]. Furthermore, Peron et al. [45] reported that TiO_2 is able to reduce the hydrogen formation during the corrosion process, which can also affect the oxidation of Sn, Eq. (1-2).

Therefore our assumption is that the reinforcement ceramics establish a protective oxide layer at the grain boundaries, which could increase the corrosion resistance of the composite solder joints. Fig. 8 shows the corrosion process in the case of a simple SAC and a composite SAC solder joint. The gray regions represent the β-Sn grains, the yellow and blue dots are the Cu_6Sn_5 and Ag_3Sn IMC particles, the green parts represent the SnO_x, and the white dots are the TiO_2 or ZnO NPs which are dispersed at the grain boundary regions. The NPs refined the β-Sn network, which is represented in Fig. 8 with smaller β-Sn grains in the composite solder joint than in the reference SAC0307. The Volta potential of Sn is much lower than IMCs, indicating that Sn is more prone to lose electrons and undergo electrochemical dissolution in thermodynamics. Besides, Yi et al. [35] found that from the perspective of corrosion kinetics, DOS calculated results suggest that the electron transfer processes of Sn are also much easier to occur relative to IMCs. Therefore, under the investigated conditions (after the condensed water film layer was formed), the initial corrosion and dissolution process will occur preferentially at β-Sn grain boundaries.

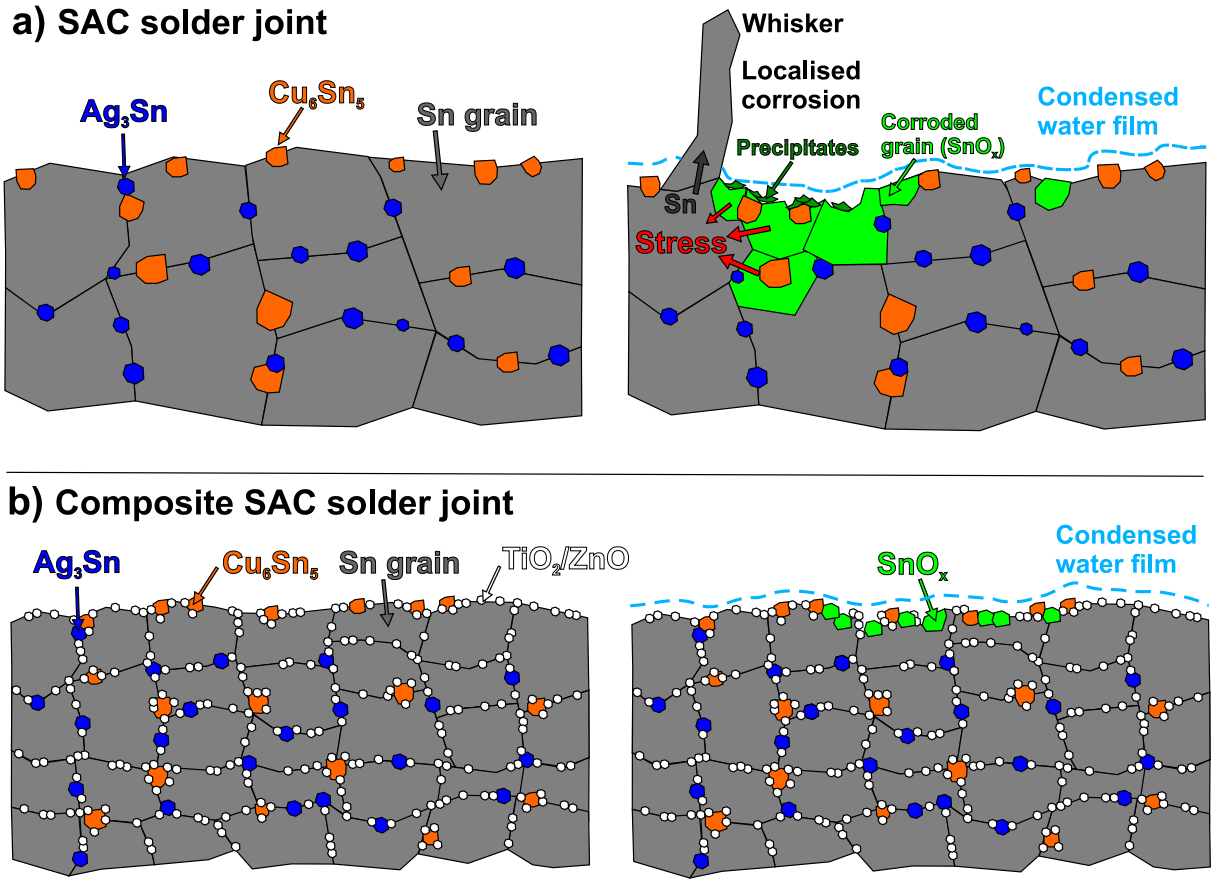

Fig. 8. Schematic illustration of corrosion process on the surface of the solder joints: a) localized corrosion SAC solder joint; b) effect of the protective oxide layer in the case of composite SAC solder joint.

In the case of a simple SAC solder joint (Fig. 8.a), the localized corrosion of Sn is progressing near IMC particles, local micro-gaps can also form [35]. The corrosion spots propagate vertically and horizontally spreading manner as well (Fig. 8.a). During the formation of SnO_x, a volumetric increase occurs in the upper region of the solder joints since the density of the SnO and SnO_2 (6.45 and 6.95 g/cm^3) is below Sn (7.31 g/cm^3). Practically, the forming SnO_x needs more space in the solder joint than the β-Sn did. Therefore, the volumetric increase causes mechanical stress on the neighbouring β-Sn grains (Fig. 8.a), which release this stress by whisker growth. That is why the Sn whiskers were usually found directly next to corrosion spots (Fig. 1).

In the case of the composite SAC solder joints (Fig. 8.b), the NP oxide ceramics (TiO_2 or ZnO) cover and protect the grain boundaries of β-Sn grains. The increased grain boundary fraction and segregation of the NPs to the grain boundaries resulted in a relatively uniform and compact (Fig. 7.c) protective oxide layer at the grain boundaries. Similarly, as Lala et al. [43]

observed in the case of the Cr addition to Sn coatings. Cr is also hardly soluble in Sn, as TiO_2 and ZnO NPs [44], so Cr was also incorporated at the β-Sn grain boundaries in the form of a protective Cr-oxide layer. Of course, the starting of the localized corrosion might not be avoided since the protective layer is not totally continuous (Fig. 8.b), but the corrosion spots could not propagate as fastly as in the case of the simple SAC solder joints. Furthermore, the possibly reduced hydrogen formation by TiO_2 NPs [45] might further slow down the corrosion of the Sn (Eq. (1-2)).

Consequently, the application of TiO_2 and ZnO NPs in 0.25wt% as reinforcement proved to be very successful in increasing the corrosion resistance of the composite solder joints and, due to this, suppressing the Sn whisker formation. However, it has to be noted that the amount of the ceramic NPs might be crucial in this application. In higher amounts (over 0.5wt%) the TiO_2 and the ZnO NPs are prone to agglomerate, which can result in deterioration of the structural integrity of the β-Sn matrix and corrosion resistance of the solder joint as well [45, 46].

5. Conclusion

The Sn whisker growth from SAC0307-TiO_2/ZnO composite solder alloys was investigated in a corrosive environment (85°C/85RH%). The main findings are the followings:

- The application of 0.25wt% TiO_2 and ZnO nano-particles as reinforcement in the SAC0307 solder alloy was very effective in suppressing the Sn whisker growth as well as the corrosion process. Even after 4000 hours of 85°C/85RH% test, the composite solder joints were almost whisker and corrosion-free. In contrast, the reference SAC0307 solder joints were covered with hundreds of nodule-type Sn whiskers and large corrosion spots. The whiskers usually developed next to the corrosion spots.
- The microstructural analysis of the Sn whiskers showed that next to the whisker root, the neighboring Sn grains were corroded and transformed to SnO or SnO_2. The transformation of β-Sn grain to SnO or SnO_2 in the localized corrosion region caused a volumetric increase in the Sn matrix since the SnO_x density is below of Sn. This volumetric increase causes mechanical stress on the neighbouring β-Sn grains, which release this stress by whisker development.
- The increased grain boundary fraction and segregation of the TiO2 and ZnO nano-particles to the grain boundaries resulted in a relatively uniform and compact protective oxide layer at the β-Sn grain boundaries. This protective layer could block the propagation of the corrosion spots and the formation of SnO_x and finally prevent the Sn whisker growth. Therefore the application of reinforcement TiO_2 and ZnO nano-

particles is favorable for increasing the reliability of SnAgCu solder joints in corrosive environments.

6. Acknowledgement

This work was partially supported by the National Research Development and Innovation Office - Hungary (NKFIH), project FK127970, and by the NRDI Fund based on the charter of bolster issued by the NRDI Office under the auspices of the Ministry for Innovation and Technology.

Data availability statement

The raw/processed data required to reproduce these findings cannot be shared at this time as the data also forms part of an ongoing study.

References

[1] Li F, Verdingovas V, Dirscherl K, Medgyes B, Ambat R. Corrosion Reliability of Lead-Free Solder Systems Used in Electronics. In Proceedings of the 2018 IMAPS Nordic Conference on Microelectronics Packaging (NordPac), Oulu, Finland, 2018, pp. 67–71. doi: 10.23919/NORDPAC.2018.8423855

[2] Krammer O, Garami T, Horvath B, Hurtony T, Medgyes B, Jakab L. Investigating the thermomechanical properties and intermetallic layer formation of Bi micro-alloyed low-Ag content solders. Journal of Alloys and Compounds. 2015; 634; 156–62.

[3] Jain N, Wang X, Jagtap P, Bower A, Chason E. Analysis of Pressure-Induced Whisker Nucleation and Growth in Thin Sn Films. Journal of Electronics Material. 2021; 50; 6639-53.

[4] Sona M, Prabhu KN. Review on microstructure evolution in Sn–Ag–Cu solders and its effect on mechanical integrity of solder joints. Journal of Material Science: Materials in Electronics. 2013; 24; 3149–69.

[5] Crandall ER, Flowers GT, Lall P, Bozack MJ, Whisker growth from Sn solder alloys. In proc. of IEEE 14th Electronics Packaging Technology Conference (EPTC), Singapore, 2012, pp. 671-675. doi: 10.1109/EPTC.2012.6507166.

[6] Illés B, Horváth B. Tin Whisker Growth from Micro-alloyed SAC Solders in Corrosive Climate, Journal of Alloys and Compounds. 2014; 616; 116–21.

[7] Illés B, Hurtony T, Medgyes B, Effect of current load on corrosion induced tin whisker growth from SnAgCu solder alloys. Corrosion Science. 2015; 99; 313-19.

[8] Hua L, Yang C. Corrosion behavior, whisker growth, and electrochemical migration of Sn–3.0Ag–0.5Cu solder doping with In and Zn in NaCl solution, Microelectronics Reliability. 2011; 51; 2274-83.

[9] Cao Z, Cao X, Sun L, He Y. Electrochemical Migration and Rapid Whisker Growth of Zn and Bi Dopings in Sn-3.0Ag-0.5Cu Solder in 3wt.% NaCl Solution, Advanced Materials Research. 2011; 239-242; 1751-60.

[10] Illés B, Hurtony T, Medgyes B, Krammer O, Dusek K, Busek D. Sn and Bi whisker growth from SAC0307-Mn07 and SAC0307-Bi1-Mn07 ultra-thin film layers. Vacuum. 2021; 187; 110121

[11] Delhaise AM, Bagheri Z, Meschter S, Snugovsky P, Kennedy J. Tin Whisker Growth on Electronic Assemblies Soldered with Bi-Containing, Pb-Free Alloys. Journal of Electronic Materials. 2021; 50; 842–54.

[12] Mohanty US, Lin K-L. Corrosion Behavior of Pb-Free Sn-1Ag-0.5Cu-XNi Solder Alloys in 3.5% NaCl Solution. Journal of Electronic Materials. 2013; 42; 628–38.

[13] Shen J, Chan YC. Research advances in nano-composite solders. Microelectronics Reliability. 2009; 49; 223-34.

[14] El-Daly AA, Fawzy A, Mansour SF, Younis MJ, Thermal analysis and mechanical properties of Sn–1.0 Ag–0.5 Cu solder alloy after modification with SiC nano-sized particles. Journal of Material Science: Materials in Electronics. 2013; 24; 2976-88.

[15] Salleh MM, McDonald S, Nogita K., Effects of Ni and TiO_2 additions in as-reflowed and annealed Sn0.7Cu solders on Cu substrates. Journal of Material Processing Technology. 2017; 242; 235–45.

[16] Ani FC, Jalar A, Saad AA, Khor CY, Ismail R, Bachok Z, Abas MA, Othman NK. SAC–xTiO_2 nano-reinforced lead-free solder joint charaexrizations in ultra-fine package assembly. Soldering and Surface Mounting Technology. 2018; 30; 1–13.

[17] Gain AK, Chan Y, Yung WK. Effect of additions of ZrO_2 nano-particles on the microstructure and shear strength of Sn–Ag–Cu solder on Au/Ni metallized Cu pads. Microelectronics Reliability. 2011; 51; 2306–13.

[18] Gain AK, Zhang L. Microstructure, mechanical and electrical performances of zirconia nanoparticles-doped tin-silver-copper solder alloys, Journal of Material Science: Materials in Electronics. 2016; 27; 7524–33.

[19] Chen G, Liu L, Silberschmidt VV, Chan Y, Liu C, Wu F. Retained ratio of reinforcement in SAC305 composite solder joints: effect of reinforcement type, processing and reflow cycle. Soldering and Surface Mounting Technology. 2016; 28; 159–66.

[20] Tang Y, Li G, Pan Y. Effects of TiO_2 nanoparticles addition on microstructure, microhardness and tensile properties of Sn–3.0Ag–0.5Cu–xTiO2 composite solder. Materials Design. 2014; 55; 574–82.
[21] Ramli M, Saud N, Salleh MM, Derman MN, Said RM, Izwan MI. Effect of TiO_2 additions on Sn-0.7Cu-0.05Ni lead-free composite solder. Microelectronics Reliability. 2016; 65; 255–64.
[22] Zhang P, Xue S, Wang J, Xue P, Zhong S, Long W, Effect of Nanoparticles Addition on the Microstructure and Properties of Lead-Free Solders: A Review, Applied Sciences. 2019; 9; 2044.
[23] Tan AT, Yusof F. Influence of nanoparticle addition on the formation and growth of intermetallic compounds (IMCs) in Cu/Sn–Ag–Cu/Cu solder joint during different thermal conditions, Science and Technology of Advanced Materials. 2015; 16; 033505.
[24] Tsao L, Chang S. Effects of Nano-TiO_2 additions on thermal analysis, microstructure and tensile properties of Sn3.5Ag0.25Cu solder. Materials Design. 2010; 31; 990–3.
[25] Lin D, Liu S, Guo T, Wang GX, Srivatsan T, Petraroli M. An investigation of nanoparticles addition on solidification kinetics and microstructure development of tin–lead solder, Material Science and Engineering A. 2003; 360; 285–92.
[25] Eid EA, Fouda AN, Duraia ESM. Effect of adding 0.5 wt% ZnO nanoparticles, temperature and strain rate on tensile properties of Sn–5.0 wt% Sb–0.5 wt% Cu (SSC505) lead free solder alloy, Material Science and Engineering A. 2016; 657; 104-14.
[27] Skwarek A, Krammer O, Hurtony T, Ptak P, Górecki K, Wroński S, Straubinger D, Witek K, Illés B. Application of ZnO nanoparticles in Sn99Ag0.3Cu0.7 based composite solder alloys, Nanomater. 2021; 11; 1545.
[28] El-Daly A, Al-Ganainy G, Fawzy A, Younis M. Structural characterization and creep resistance of nano-silicon carbide reinforced Sn–1.0Ag–0.5Cu lead-free solder alloy. Material. Designe. 2014; 55; 837–45.
[29] Shi Y, Liu J, Xia Z, Lei Y, Guo F, Li X. Creep property of composite solders reinforced by nano-sized particles, Journal of Material Science: Materials in Electronics. 2007; 19; 349–56.
[30] Salleh MAAM, Al Bakri AMM, Kamarudin H, Bnhussain M, Somidin F. Solderability of Sn-0.7Cu/Si3N4 lead-free composite solder on Cu-substrate. Physics Procedia. 2011; 22; 299–304.

[31] Fawzy A, Fayek S, Sobhy M, Nassr E, Mousa M, Saad G. Tensile creep characteristics of Sn–3.5Ag–0.5Cu (SAC355) solder reinforced with nano-metric ZnO particles. Material Science and Engineering A. 2014; 603; 1-10.

[32] Krammer O, Illés B, Bátorfi R, Dušek K. Automatic characterisation method for statistical evaluation of tin whisker growth. Microelectronics Reliability. 2017; 73; 14-21.

[33] Lixia Y, Zhenghui L, Ke W, Xiupeng L, Guixiang W, Effect of TiO_2 Sol on the Microstructure and Tribological Properties of Cu-Sn Coating, Rare Metal Materials and Engineering. 2017; 46; 2801–6.

[34] Cho S, Yu J, Kang SK, Shih D-Y. Oxidation Study of Pure Tin and Its Alloys via Electrochemical Reduction Analysis. Journal of Electronic Materials. 2005; 34; 635–42.

[35] Yi P, Dong C, Xiao K, Li X. Study on corrosion behavior of β-Sn and intermetallic compounds phases in SAC305 alloy by in-situ EC-AFM and first-principles calculation, Corrosion Science. 2021; 181; 109244.

[36] Horváth B, Shinohara T, Illés B. Corrosion Properties of Tin-Copper Alloy Coatings in Aspect of Tin Whisker Growth, Journal of Alloys and Compounds. 2013; 577; 439-44.

[37] Séby F, Potin-Gautier M, Giffaut E, Donard O. A critical review of thermodynamic data for inorganic tin species. Geochimica et Cosmochimica Acta. 2001; 65; 3041–53.

[38] Chen G, Wang XH, Yang J, et al., Effect of micromorphology on corrosion and mechanical properties of SAC305 lead-free solders, Microelectronics Reliability. 2010; 108; 113634–50.

[39] Gupta A, Srivastava C. Low-temperature Sn electrodeposition: Texture evolution, grain boundary constitution and corrosion behavior, Surface and Coating Technology. 2021; 425; 127709.

[40] Tsuji K. Roll of Grain-boundary Free Energy & Surface Free Energy for Tin Whisker Growth, Proc. of the IPC/JEDEC 4th Intl. Conf. on Lead-Free Electronic Components and Assemblies. 2003.

[41] Gupta A, Srivastava C, Temperature driven texture and grain boundary engineering of electrodeposited β-Sn coatings and its effect on the coating corrosion behaviour: Five-parameter grain boundary character distribution analysis study. Scripta Materiallia. 2021; 196; 113763.

[42] Gupta A, Srivastava C, Electrodeposition current density induced texture and grain boundary engineering in Sn coatings for enhanced corrosion resistance. Corrosion Science. 2022; 194; 109945.

[43] Lala SRF, Jyotheender KS, Gupta A, Arora S, Kumar P, Srivastava C. Evolution of texture and strain in Sn coating with Cr addition and its effect on the coating corrosion behavior. Materialia. 2020; 14; 100944.

[44] Rashidi R, Naffakh-Moosavy H. Metallurgical, physical, mechanical and oxidation behavior of lead-free chromium dissolved Sn–Cu–Bi solders. Journal of Materials Research and Technology. 2021; 13; 1805-25.

[45] Peron M, Bertolini R, Cogo S, On the corrosion, stress corrosion and cytocompatibility performances of ALD TiO_2 and ZrO_2 coated magnesium alloys. Journal of the mechanical behavior of biomedical materials. 2022; 125; 104945.

[46] Ying LX, Wu K, Li DY, Wu CX, Fu Z. TiO_2 Sol strengthened Cu-Sn-PTFE composite coatings with high homogeneity and superior resistance to wear. Wear. 2019; 426–427; 258–64.